Nonperturbative Visualization of Nanoscale Plasmonic Field Distributions via Photon Localization Microscopy

A. McLeod, A. Weber-Bargioni, Z. Zhang, S. Dhuey, B. Harteneck, J. B. Neaton, S. Cabrini, and P. James Schuck

Phys. Rev. Lett. **106**, 037402 — Published 18 January 2011

DOI: 10.1103/PhysRevLett.106.037402

Non-perturbative visualization of nanoscale plasmonic field distributions via photon localization microsocopy

P. James Schuck[1†*], A. McLeod[1†], A.Weber-Bargioni[1], Z. Zhang[2], S. Dhuey[1], B. Harteneck[1], J. B. Neaton[1*], S. Cabrini[1]

[1]Molecular Foundry, Lawrence Berkeley National Lab, Berkeley, CA 94720

[2]Department of Chemistry, UC Berkeley, Berkeley, CA 94720

[†]These authors contributed equally to this work

*pjschuck@lbl.gov, jbneaton@lbl.gov

PACS Numbers: 78.67.-n, 78.55.-m, 42.65.-k, 78.67.pt

Abstract:

We demonstrate the non-perturbative use of diffraction-limited optics and photon localization microscopy to visualize the controlled nanoscale shifts of zeptoliter mode volumes within plasmonic nanostructures. Unlike tip- or coating-based methods for mapping near-fields, these measurements do not affect the electromagnetic properties of the structure being investigated. We quantify the local field manipulation capabilities of asymmetric bowtie antennas, in agreement with theoretical calculations. The photon-limited localization accuracy of nanoscale mode positions is determined for many of the measured devices to be within a 95% confidence interval of +/- 2.5 nm. This accuracy also enables us to characterize the effects of nm-scale fabrication irregularities on local plasmonic mode distributions.

The desire for ultrafast manipulation of deeply sub-wavelength electromagnetic fields has spurred significant investigation into plasmonic nanostructure properties and device design. However, due to the nanoscale nature of many plasmon-related quantities, experimental characterization of such structures presents a unique set of challenges. Specifically, non-perturbative measurements of the spatial distributions of local fields have proven especially elusive, both because structure feature sizes are below the diffraction limit and because modal characteristics are extremely sensitive to their local environment. Current techniques for mapping plasmonic near-fields and their movements involve using a probe tip apex for scattering/collecting local fields [1], or coating the structures with optically- or thermally-active media and inducing chemical and/or structural changes wherever the fields are strongest [2]. These methods are not ideal, as they require placing a foreign object or material into the sensitive near-fields, necessarily perturbing the properties of the studied nanostructure [3].

In this work, we demonstrate the non-perturbative use of diffraction-limited nonlinear optics and photon localization microscopy to visualize the nanometer-scale controlled shifts of zeptoliter mode volumes within plasmonic nanostructures [4]. As a proof of concept, we image the local energy-dependent changes in near-field distributions within individual gold asymmetric bowtie nano-colorsorters (ABnCs) [5], a class of plasmonic color sorters [6] based on the "cross" nanoantenna geometry [7]. These devices are specifically engineered to not only capture and confine optical fields, but also to spectrally filter and steer them while maintaining nanoscale field distributions. Their spectral properties, including Fano-like resonances [8], and localized spatial mode distributions can be readily tuned by controlled asymmetry, and each of the zeptoliter

mode volumes within an ABnC, spatially separated by only tens of nm, can be individually addressed simply by adjusting the incident wavelength [5].

To image the modes, we collect the two-photon photoluminescence (TPPL) signal [9,10] from the ABnCs when excited by a pulsed titanium sapphire laser tuned to a mode resonance (in a sample-scanning confocal modality; details in the supplemental information (SI) [11]). The TPPL originates from the interaction of the intrinsic local field with the Au nanostructure itself and therefore involves no external perturbation of the device or its local environment. TPPL has previously been used to measure plasmonic field properties such as enhancement and near-field resonance [10,12], as well as mode distributions with diffraction-limited spatial resolution [13].

Recently, photon localization microscopy has gained significant attention within the molecular and cellular imaging communities due to its ability to determine the position of a single emitter with nanoscale accuracy. A more detailed discussion can be found in [14] and references therein. By applying photon localization microscopy centroid analysis [15] to TPPL data from plasmonic systems, we can determine the center position of a local field mode in the same way, separately localizing nanoscale plasmon modes within the same diffraction-limited focal volume. For our sample-scanning confocal TPPL images of the ABnCs, the position accuracy is limited primarily by the number of TPPL photons we collect, and we demonstrate here a 95% confidence interval accuracy of +/- 2.5 nm.

The asymmetry in our ABnCs is created by moving the "vertical" bowtie component of a cross nanoantenna right-of-center, thereby reducing the cross symmetry from C_{4v} to C_s. We have previously shown that, due to complex coupling within the

ABnC, this shift breaks the nanoantenna's primary plasmon resonance into two spatially and spectrally distinct modes: a higher-energy "blue" mode confined near the tip of the more isolated triangle on the left, and a lower-energy "red" mode primarily confined near the smaller gaps on the other side (Fig. 1) [5]. The two mode volumes are spatially separated by a distance significantly below the diffraction limit (demonstrated below).

The ABnCs are engineered to have the "blue" resonance near 780 nm and the "red" resonance near 840 nm. They are fabricated using electron-beam lithography and consist of ~18-nm-thick Au on top of a 2 nm Ti adhesion layer. More fabrication details are given in [11]. Our samples consist of arrays of single ABnCs (fig. 1), with shifts of the vertical bowtie component ranging from 4 nm to 15 nm right-of-center. Associated with each ABnC structure is a Au disk dimer (nominal disk diameters = 100 nm, gap = 15 nm), which acts as fiduciary mark for the TPPL localization microscopy analysis. Simulations are performed using the open-source finite-difference time-domain (FDTD) code MEEP [16] via the interactive analysis suite Molecular Foundry PhotonicsTK, hosted online at www.nanoHUB.org [17] (see SI [11] for simulation details).

In our experiment, A 100X, 0.95 numerical aperture microscope objective is used for both excitation and TPPL collection. The collected broadband TPPL is detected by an avalanche photodiode (APD) after passing through spectral filters (details in SI). We collect TPPL images of individual ABnCs and their associated fiduciary marks while first exciting at 780 nm, then again at 840 nm. This sequence is repeated to assure reproducibility, and care is taken to operate at power densities below the damage threshold [10]. By exciting the local modes at different times, we combine the

localization data from different images to yield information that is significantly better than the diffraction limit.

TPPL images of the fiduciary marks are centered at the disk-dimer gap for both excitation wavelengths. On the other hand, TPPL images of the ABnC should have a center position that depends on which resonance is excited [18]. The "blue resonance" TPPL centroid is expected to be located closer to the left-most triangle in the ABnC, while at the "red" resonance, the TPPL image center will be shifted to the right. The size of the shift is related to the offset of the vertical bowtie component.

Because the TPPL images are collected serially while raster scanning the sample, the scan direction is chosen such that each ABnC and its related fiduciary mark are imaged within the same scan lines, thereby limiting potential error in localization accuracy due to drift during image acquisition. By scanning through our focused laser spot and collecting all generated TPPL signal, we are primarily measuring the excitation response functions of our nanoantennae, convolved with the point spread function (PSF) of our optical system. Complementary information can be gained by exciting and collecting TPPL images in a widefield modality as a function of incident and/or emission energy.

Once TPPL intensity images are collected, they are fit to two-dimensional Gaussians (Fig. 1f), and center positions and associated confidence intervals are calculated. The nanoscale shifts of the two modes within each ABnC are then determined by calculating the center positions of the ABnC images relative to those of the fiduciary mark. Localization accuracy depends both on the fits of the ABnC images *and* the disk-dimer images. For our Au structures, TPPL is stronger for higher-energy

excitation, so the localization accuracies are better for 780 nm modes than for 840 nm modes. As experimental controls, single bowties and individual triangles were also fabricated on the sample and imaged in the same way. As expected, no appreciable mode shift is measured from these structures (see SI Fig. S2 [11]).

After optical measurements, all structures are imaged in the SEM to determine their actual geometries, including the extent of the asymmetry of each ABnC. The results of the localization microscopy analysis for each structure are then correlated with these quantities. In Figure 2a, the relative center positions of an ABnC's two modes as determined by the TPPL image centroid analysis are shown, overlaid on its SEM image. We have estimated the position of the optical data relative to the ABnC SEM based on simulation. In this case, the 8 nm vertical-bowtie offset of the ABnC has led to a measured shift of 32 nm in the centers of the TPPL images at the two distinct plasmon modes. The center positions have been determined with 95% confidence interval accuracies of 2.5 nm (780 nm excitation) and 11.3 nm (840 nm excitation). The relatively poor center position accuracy of the "red" mode is due mostly to the weak TPPL signal arising from the fiduciary mark at 840 nm excitation. This experimentally-determined shift in mode position corresponds well with the calculated $|E|^4$ centroid positions (Fig. 2b-c). Data from this structure is also shown in Fig. 3 as the experimental data point at asymmetry parameter = 0.22.

Importantly, because of the nm-scale accuracy of the localization measurements, one can observe the effects of fabrication variations on local mode distributions, an example of which is shown in Fig. 2d-f and Fig. 3. Although each ABnC is nominally designed to have C_s symmetry with a reflection axis along the x-axis, variations occur

due to fabrication limitations at these length scales. In Fig. 2(d), the bottom triangle in the ABnC was offset in both the x- and y-directions by a few nm. These relative offsets are theoretically expected to lead to localized plasmon distributions that are also displaced in x and y relative to one another. This is consistent with our measurements (see Fig. 2d-f): the red mode TPPL centroid exists primarily near the smallest gap in the ABnC [5], which is both to the right and down from the blue mode TPPL centroid.

The change in the relative positions of the local modes can be controlled by the degree of vertical bowtie offset in the ABnC. Using TPPL localization microscopy, we have measured the relative spatial shifts of ABnC mode positions for offsets ranging from 4 nm to 15 nm. These shifts are plotted in Fig. 3 as a function of a normalized asymmetry parameter defined as the vertical bowtie offset divided by the measured gap size of the horizontal bowtie component. A clear relationship between the amount of asymmetry and spatial shift between modes is demonstrated and agrees well with the theoretically predicted values. Details of the theoretically calculated shifts are discussed in the SI [11]. In Fig. 3, scatter of the experimental data around the theoretical curve is real and highlights the precision of the optical measurements. The scatter is due to fabrication-limited variations in actual device structure relative to the more ideal theoretically modeled cases (see discussion in [11] and Fig. S4). This optical technique is complementary in many ways to the recently demonstrated electron-based plasmon imaging techniques [19], and both lend new insights into localized light-matter interactions. The notable advantage of the electron-based techniques is that they can give a full, nanoscale resolution image of the spatial distribution of the mode, and some modalities allow for full wide-field imaging. Also, localization accuracies associated

with electron-based techniques can be orders-of-magnitude higher than for optical methods. Key advantages of this optical technique are the direct probing of photon-structure coupling and its experimental accessibility, simplicity, and throughput, making it appealing not only for basic investigations in research labs but also for characterization and metrology in more industrial/development settings. Additionally, the all-optical technique can be performed in virtually all possible sample environments (ambient, liquid, vacuum, etc).

In conclusion, we have developed a technique for imaging local plasmonic nearfield distribution positions that, unlike current methods, does not perturb the electromagnetic properties of the investigated nanostructure. Our nanoscale imaging of zeptoliter mode volume positions corresponds well with FDTD simulations, and we have demonstrated a photon-limited localization accuracy of less than 2.5 nm. In addition, we have shown that by increasing the asymmetry and controlling the gap sizes between the constituent parts of the ABnC, we can tune the relative positions of the local modes with nm-scale accuracy. Ultimately, we believe the information contained within images of this type can be used to elucidate multiple mode-specific interactions between light and plasmonic nanostructures.

Acknowledgments: We thank S.W. Wu, Y. Hu, and colleagues at Molecular Foundry and UC Berkeley for their gracious help and discussions. Work at the Molecular Foundry was supported by the Office of Science, Office of Basic Energy Sciences, of the U.S. Department of Energy under Contract No. DE-AC02-05CH11231. We acknowledge use of nanoHUB.org resources provided by the Network for Computational Nanotechnology funded by the National Science Foundation.

Figure Captions:

Figure 1 (color online). (a-b) Calculated images of the spatially and spectrally distinct near-field $|E|^2$ distributions surrounding an ABnC when excited at (a) the higher-energy "blue" mode, and (b) the lower-energy "red" mode. Scanning electron microscope (SEM) images of a representative (c) ABnC and (d) associated disk-dimer fiduciary mark. TPPL images of the structures in (c-d) are shown in (e). (f) Two-dimensional Gaussian fits of the TPPL images in (e). Standard deviations of these fits are (σ_x = 151.5 nm, σ_y = 154.3 nm) for the upper spot and (σ_x = 136.3 nm, σ_y = 129 nm) for the lower spot in (f).

Figure 2 (color online). The measured mode positions for an ABnC with approximate Cs symmetry are overlaid in (a) on its SEM image. The centroid of the "blue" mode image is marked by a blue "X" and the center position of the "red" mode image is marked by a red "X". The center positions are known with accuracies given in the text. Theoretically modeled positions of the $|E_{Au}|^4$ centroids are shown in (b) for blue mode and (c) for red mode excitation. The color values in (b-c) and (e-f) correspond to near-field $|E|^2$ values on a log scale. Center positions from a more asymmetric ABnC (offsets of the constituent triangles are in both x- and y-directions) are shown in (d). Calculated $|E_{Au}|^4$ centroid positions for the ABnC in (d) are plotted in (e) and (f) for blue and red mode excitation, respectively.

Figure 3 (color online). TPPL image centroid shifts plotted as a function of normalized offset of the vertical bowtie component in the +x direction. Experimentally measured values are marked by red circles and FDTD-calculated values are shown by the blue line

and circles. The error bars correspond to the one-sigma accuracy of the experimentally determined shifts along the x-axis.

Figure 1:

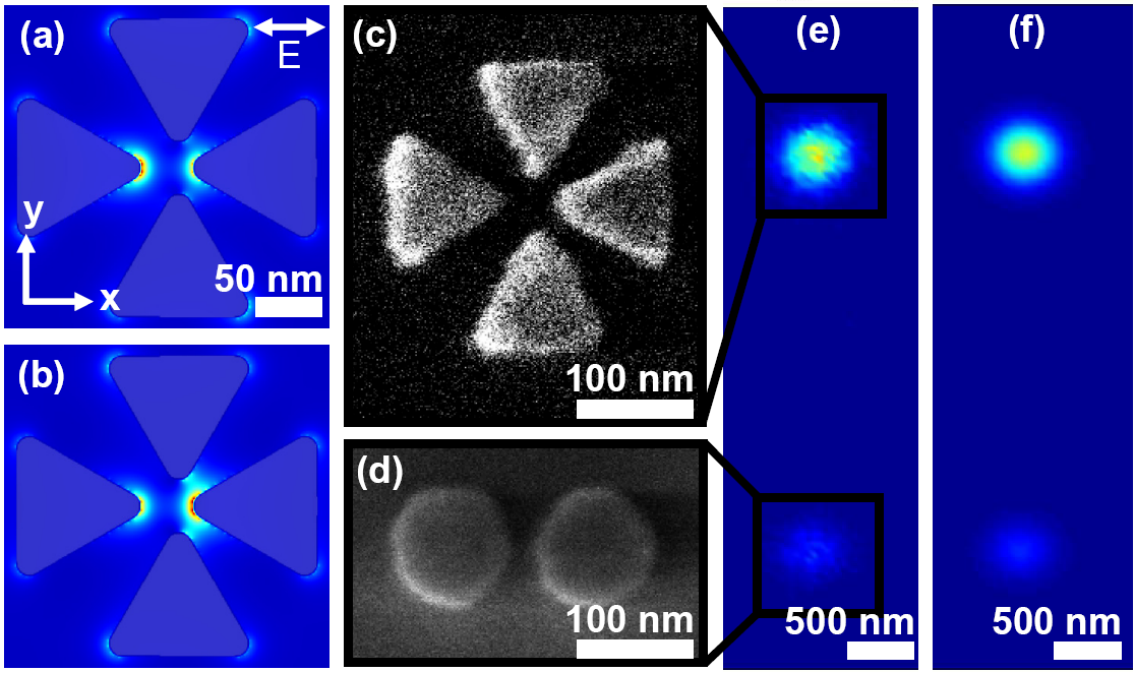

Figure 2.

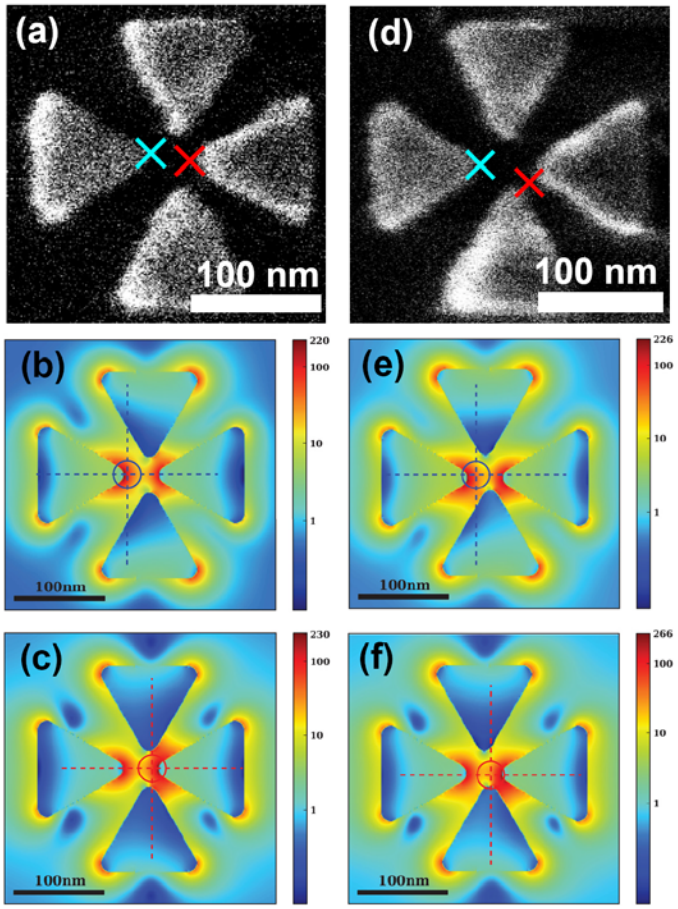
(a)
100 nm
(d)
100 nm
(b)
220
100
10
1
100nm
(e)
226
100
10
1
100nm
(c)
230
100
10
1
100nm
(f)
266
100
10
1
100nm

Figure 3.

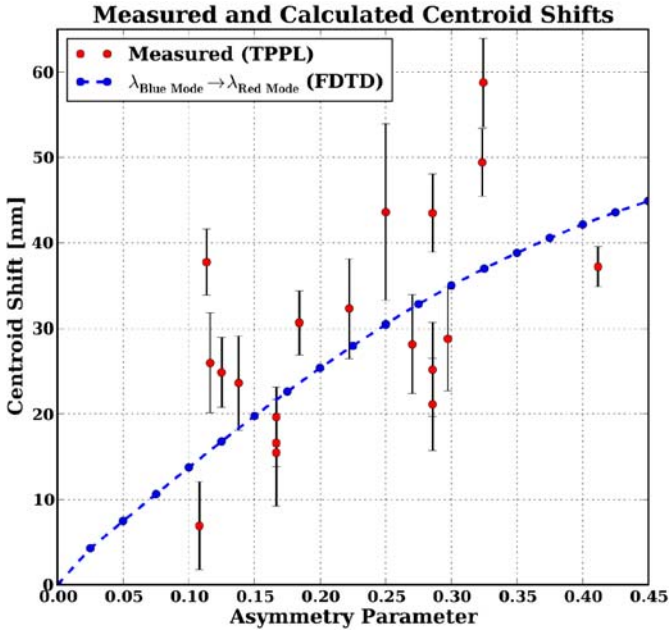
Measured and Calculated Centroid Shifts
Measured (TPPL)
$\lambda_{\text{Blue Mode}} \rightarrow \lambda_{\text{Red Mode}}$ (FDTD)
Centroid Shift [nm]
Asymmetry Parameter
0
10
20
30
40
50
60
0.00
0.05
0.10
0.15
0.20
0.25
0.30
0.35
0.40
0.45

References:

[1] M. Rang *et al.*, Nano Lett. **8**, 3357 (2008); F. Keilmann and R. Hillenbrand, Philos. Trans. R. Soc. Lond. Ser. A-Math. Phys. Eng. Sci. **362**, 787 (2004); K. G. Lee *et al.*, Nature Photon. **1**, 53 (2007); R. L. Olmon *et al.*, Opt. Express **16**, 20295 (2008); M. Schnell *et al.*, Nature Photon. **3**, 287 (2009); D. S. Kim *et al.*, Nano Lett. **9**, 3619 (2009); E. Verhagen *et al.*, Phys. Rev. Lett. **102**, 203904 (2009); R. Zia, J. A. Schuller, and M. L. Brongersma, Phys. Rev. B **74**, 165415 (2006); R. Guo *et al.*, Opt. Express **18**, 4961 (2010).

[2] A. Sundaramurthy *et al.*, Nano Lett. **6**, 355 (2006); L. Rontzsch *et al.*, Appl. Phys. Lett. **90**, 044105 (2007); S. Nah *et al.*, J. Phys. Chem. C **114**, 7774 (2010); T. Grosjean and D. Courjon, Opt. Express **14**, 2203 (2006).

[3] S. Zhang *et al.*, Opt. Express **18**, 6048 (2010).

[4] M. I. Stockman, Phys. Rev. Lett. **93**, 137404 (2004); H. Wang *et al.*, PNAS **103**, 10856 (2006); J. A. Fan *et al.*, Science **328**, 1135 (2010).

[5] Z. Zhang *et al.*, Nano Lett. **9**, 4505 (2009).

[6] E. Laux *et al.*, Nature Photon. **2**, 161 (2008); A. V. Malyshev, V. A. Malyshev, and J. Knoester, Nano Lett. **8**, 2369 (2008); Z. Kang and G. P. Wang, Opt. Express **16**, 7680 (2008); B. Lahiri *et al.*, Opt. Express **17**, 1107 (2009).

[7] P. Biagioni *et al.*, Phys. Rev. Lett. **102**, 256801 (2009).

[8] N. Verellen *et al.*, Nano Lett. **9**, 1663 (2009).

[9] G. T. Boyd, Z. H. Yu, and Y. R. Shen, Phys. Rev. B **33**, 7923 (1986); M. R. Beversluis, A. Bouhelier, and L. Novotny, Phys. Rev. B **68**, 115433 (2003); P. Biagioni *et al.*, Phys. Rev. B **80**, 045411 (2009).

[10] P. J. Schuck *et al.*, Phys. Rev. Lett. **94**, 017402 (2005).

[11] See EPAPS Document No. [number will be inserted by publisher] for supporting information.

[12] D. ten Bloemendal *et al.*, Plasmonics **1**, 41 (2006); T. Sondergaard *et al.*, Nano Lett. **10**, 291 (2010).

[13] P. Ghenuche, S. Cherukulappurath, and R. Quidant, New J. Phys. **10**, 105013 (2008); P. Ghenuche *et al.*, Phys. Rev. Lett. **101**, 116805 (2008); J.-S. Huang *et al.*, Nano Lett. **10**, 2105 (2010).

[14] W. E. Moerner, Proceedings of the National Academy of Sciences **104**, 12596 (2007).

[15] R. J. Ober, S. Ram, and E. S. Ward, Biophys. J. **86**, 1185 (2004); R. E. Thompson, D. R. Larson, and W. W. Webb, Biophys. J. **82**, 2775 (2002).

[16] A. F. Oskooi *et al.*, Comput. Phys. Commun. **181**, 687 (2010).

[17] "Nanophotonics Toolkit" http://nanohub.org/resources/photonicstk, (2010).

[18] A. I. Denisyuk *et al.*, Nano Lett. **10**, 3250 (2010).

[19] A. Kubo *et al.*, Nano Lett. **5**, 1123 (2005); T. Schmidt *et al.*, Ultramicroscopy **110**, 1358 (2010); R. Vogelgesang and A. Dmitriev, The Analyst **135**, 1175 (2010); F. J. Garcia de Abajo, Reviews of Modern Physics **82**, 209 (2010).